

Article

Surface Roughness Effects on the Properties of Silicon-Doped Diamond-like Carbon Coatings

Katarzyna Piotrowska, Monika Madej *, Joanna Kowalczyk and Krystyna Radoń-Kobus

Department of Mechatronics and Mechanical Engineering, Kielce University of Technology, 25-314 Kielce, Poland; kpawelec@tu.kielce.pl (K.P.); jkowalczyk@tu.kielce.pl (J.K.); kradonkobus@tu.kielce.pl (K.R.-K.)

* Correspondence: mmadej@tu.kielce.pl

Abstract: This paper evaluates surface roughness effects on the properties of a-C:H:Si coatings obtained using plasma-assisted chemical vapor deposition (PACVD). Prior to coating deposition, the surfaces of the samples were subjected to grinding ($R_a = 0.25$) and then polishing ($R_a = 0.05$) or sandblasting ($R_a = 1.41$). Microscopic observations, measurements of thickness, wettability, surface topography, and tribological tests were used to characterize the substrate. The coating microstructure, thickness, and chemical content were investigated using scanning electron microscopy with energy dispersive spectroscopy (EDS). The geometric structure of the surface was examined using confocal microscopy before and after tribological tests. Tribological studies used a ball-on-disk sliding configuration in reciprocating motion under dry friction and cutting oil lubrication. The values of the contact angles were indicative of surface hydrophilic characteristics. Compared with the sandblasted surfaces, the adhesion strength of the coatings deposited on the polished surfaces was found to be higher. The coatings contributed to the improvement of friction and wear parameters. Under dry friction, a-C:H:Si coating friction coefficients and linear and volumetric wear on the polished surface were reduced compared with the sandblasted surface, respectively, by 10%, 83%, and 85%. In addition, the lubricant contributed to reducing the friction coefficients of the coating applied to the sandblasted sample compared with the polished sample without the coating by about 94%. Microscopic observations of wear traces allowed the determination of wear mechanisms; in the case of Ti13Nb13Zr, it was tribochemical wear through oxidation, while in the case of coatings, scratching and microcutting dominated.

Keywords: diamond-like carbon; wettability; adhesion; surface texture; friction; wear



Citation: Piotrowska, K.; Madej, M.; Kowalczyk, J.; Radoń-Kobus, K. Surface Roughness Effects on the Properties of Silicon-Doped Diamond-like Carbon Coatings. *Coatings* **2023**, *13*, 1629. <https://doi.org/10.3390/coatings13091629>

Academic Editor: Ludmila B. Boinovich

Received: 9 August 2023

Revised: 12 September 2023

Accepted: 15 September 2023

Published: 17 September 2023



Copyright: © 2023 by the authors. Licensee MDPI, Basel, Switzerland. This article is an open access article distributed under the terms and conditions of the Creative Commons Attribution (CC BY) license (<https://creativecommons.org/licenses/by/4.0/>).

1. Introduction

Recent years have seen an increased demand for titanium and its alloys in various sectors of the economy. The great interest in these materials results primarily from their high specific strength, low density, heat resistance and cracking resistance at low temperatures, and excellent corrosion resistance under operating conditions. Titanium alloys are used to produce, among others, compressor blades, wheel support beams, heat exchangers, condensers, desalination systems, profiling tools, valves, and other machine parts. The limitation of using titanium alloys for machine and device components is their low hardness and resistance to abrasive wear [1,2].

Wear is a process that occurs on interacting elements of machines and devices in motion. Most often, it is mechanical in nature. Less often, it is mechanical combined with the chemical action of the surrounding medium [3].

The resistance of a material to wear is dependent on the topography of its outermost layer obtained in a technological process. The author of [4] defines the top surface as a set of components comprising the surface physicochemical (microstructure, its mechanical and physicochemical properties) and stereometric (roughness, shape deviation and flaws) characteristics. Since all these components affect the service life of machine elements

and depend on many factors, e.g., material properties, finishing technology, functional properties of the produced surface, and operating conditions [5,6], the element surface is a key player in machine operation. Surfaces are subject to modification due to friction, external forcing, and impact time. The initial values of stereometric and physicochemical parameters change to produce an operational surface layer [4]. Closely related to the concept of friction is the phenomenon of wear. It occurs on the surface layers of interacting solids, leading to changes in the structure and physicochemical properties of sliding elements, their dimensions, shape, and mass loss [7,8].

In machine parts, the predominant type of interaction between two or more components is sliding friction, with abrasive wear as the main wear type (Figure 1) [9,10].

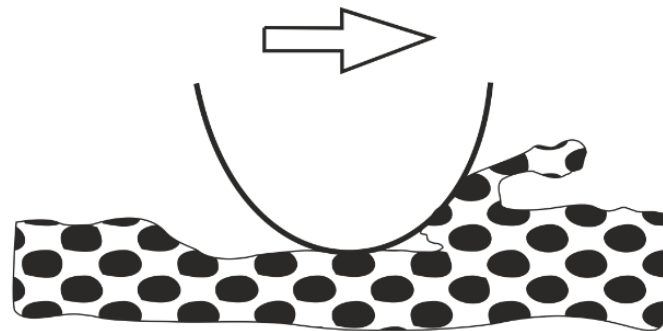


Figure 1. Abrasive wear scheme.

According to Plaza et al. [11], abrasive wear dominates under dry friction and comprises about 80%–90% of all tribological wear. It is most often formed as a result of the movement of wear products (hard abrasive particles between frictionally interacting elements). To counteract wear, surface layers are modified or lubricants suitable for a given technical application are used. Antiwear technologies are gathering momentum with their capability of enhancing the durability of components operating under variable tribological and non-tribological loads. Antiwear technologies find applications across diverse areas, such as tooling, automotive production, chemical industry, food processing, medicine, and others [12,13]. In many industrial applications, commonly used conventional technologies do not meet the requirements for modern machinery and equipment components.

Surface engineering techniques based on unconventional technologies, such as electrochemical and chemical deposition [14], electrical discharge machining and laser beam machining [15–18], increasingly popular 3D printing [19], modern coating-forming methods based on physical and chemical vapor deposition (PVD, CVD) [12–14], and ion implantation [20], are making a significant impact. Advanced surface-coating techniques enable a large range of surface modifications in order to obtain the functional properties, including tribological properties of the top layer. Various surface modification techniques (polishing, sandblasting, etching), ion implantation, or deposition of thin hard coatings are available [21–24]. Examples include diamond-like carbon (DLC) coating type a-C:H characterized by high hardness due to sp^3 bonds (typical in diamond) and excellent lubrication properties due to sp^2 bonds (typical in graphite) [25–29].

DLC coatings display excellent mechanical properties, such as high elastic modulus, resistance to brittle fracture, and chemical stability. These characteristics allow them to be used in tribological systems where a low coefficient of friction and high resistance to friction wear are required, i.e., in the transportation equipment, tooling, textile, medical, and plastics processing industries [30,31].

The challenging downside of DLC coating properties is high residual stress, which can inhibit the coating adhesion to the substrate. To prevent this, intermediate layers are deposited, or the coatings are doped with other elements [32–36].

Research conducted by Kim et al. [37] indicated that non-lubricated friction nodes with Si-DLC may have lower friction coefficients than DLC and that friction coefficients decrease

with increasing Si content in DLC. Research by [38] proved that Si-DLC friction pairs exhibited lower wear when lubricated with a lubricant used in belt conveyors. Moreover, according to [39], the addition of Si improved the adhesion and increased the thermal stability of DLC layers. In [40], the authors examined the tribological properties of diamond-like coatings and coatings doped with silicon and tungsten. The tests were carried out in reciprocating motion, without lubrication, and with an amplitude of 1, 6, and 36 Hz. The test results indicated that, when using an amplitude of 1 and 6 Hz, the Si-DLC coating was characterized by lower average friction coefficients than DLC and W-DLC.

DLC coatings can be obtained by chemical vapor deposition (CVD) [1,32,41] or hybrid methods that use the CVD process characteristics. In the process, chemical compounds (known as precursors) are introduced into the reaction chamber in the form of a gas activated to become more reactive and then deposited on the substrate as a thin film. CVD techniques require the use of high temperatures, 900–1100 °C or higher, in order for the reactants to decompose properly and for chemical reactions to proceed. This significantly limits their application range, for example, on components subjected to dynamic operational loads [2]. Plasma enhancement of the conventional CVD process produces a plasma-assisted chemical vapor deposition (PACVD) technique that allows the lowering of the deposition temperature to <250 °C [42]. The innovative coating manufacturing techniques produce surfaces with improved mechanical and tribological properties for an increased service life of machine and equipment components [43].

The literature analysis indicates that no research has been conducted on assessing the effects of surface treatments such as polishing and sandblasting or a-C:H:Si coatings on the properties of titanium alloys. Therefore, this study attempted to examine their influence on the properties of the Ti13Nb13Zr alloy. Surface geometry, as well as mechanical and physicochemical properties, were comprehensively characterized. The essential element of this study was the assessment of the applied treatments on the tribological properties of the titanium alloy under dry friction and BeCool Met 3920 coolant lubricated friction. No reports on using the proposed lubricant have been published in the literature. In addition, wear mechanisms occurring between interacting elements were determined.

The test results showed that surface treatments and antiwear coatings on friction pair elements, additionally supported by a lubricant, reduced the intensity of wear of the Ti13Nb13Zr titanium alloy.

2. Materials and Methods

2.1. Preparation of Titanium Samples

The tests used Ti13Nb13Zr titanium alloy, purchased in the form of a rod with a diameter of 30 mm, the chemical composition as in Table 1. Titanium alloy has good mechanical properties and corrosion resistance [26,44,45].

Table 1. Chemical composition of Ti13Nb13Zr titanium alloy.

Ti13Nb13Zr, % Content							
Ti	Nb	Zr	Fe	C	N	O	H
Balance	13.15	12.99	0.02	0.005	0.01	0.053	0.001

Surface preparation was a key stage before coating application. Disc samples with a diameter of 30 mm and a height of 6 mm were ground and then polished (a) with a FEMTO 1100 Pace Technologies polisher and sandblasted (b). The grinding process used silicon carbide abrasive papers with progressively increasing grit sizes from 120 to 2500 µm. The samples were polished on cloth with an Al₂O₃ polishing slurry with a grain size of 0.05 µm. For sandblasting, an Al₂O₃ grain size of 125 µm was used. The surface roughness expressed by the Ra parameter for the polished sample was 0.05 µm, while that of the sandblasted sample was about 1.41 µm. Photographs of the samples prior to coating application are shown in Figure 2.

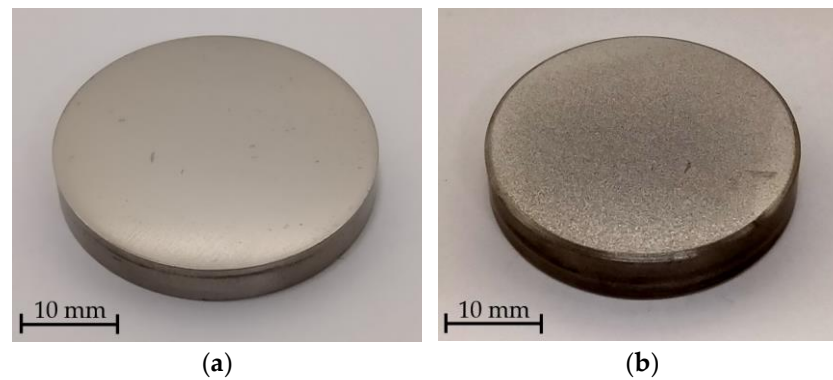


Figure 2. Samples after treatments: polishing (a) and sandblasting (b).

The so-prepared surfaces were cleaned in an ultrasonic cleaning line using ethanol. The diamond-like coating type a-C:H doped with silicon (a-C:H:Si) was applied by plasma-assisted physical vapor deposition (PACVD) at <220 °C. A schematic of the process is shown in Figure 3. In the process, argon and methane gases were introduced into the vacuum chamber, where the plasma was ionized, and the particles diffused toward the material. Plasma was produced by applying an electric field to a volume of gas using an RF glow discharge. The coupling created between the electrodes caused gases to settle on the substrate and form a coating.

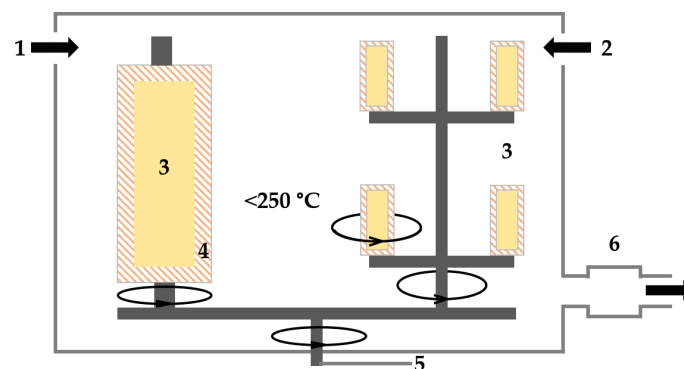


Figure 3. Schematic of the PACVD system [46]. (1) Argon, (2) reactive gas, (3) components/tools, (4) planar magnetron evaporation source (coating material), (5) high-frequency connection, (6) vacuum pump.

The carbon layers were made in Oerlikon Balzers using a RS50. Views of the polished (a) and sandblasted (b) coated samples are shown in Figure 4.

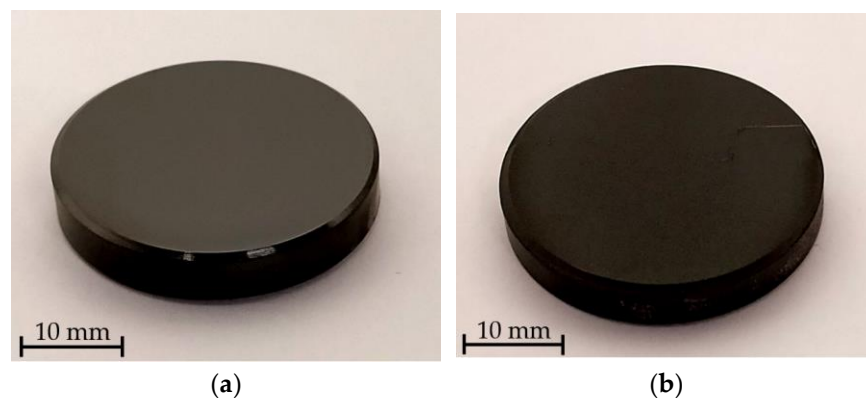


Figure 4. Coated samples: polished (a) and sandblasted (b).

2.2. Research Methodology

The most important parameter proving the functionality of coatings is their adhesion to the substrate. The micro combi tester (MCT3) from Anton Paar (MCT³) and the scratch test were used to determine it. The test consisted of generating a scratch with a Rockwell diamond indenter (Figure 5) on a-C:H:Si coatings deposited on different surfaces (polished and sandblasted) over a distance of 3 mm. A loading force of 15 N and a scratching speed of 12 mm/min were applied during the test. The use of advanced Scratch software (version 8.0.19) allowed real-time recording of the most important test parameters: coefficient of friction, depth of indenter penetration, and acoustic emission. The results of these tests are presented in Section 3.1.

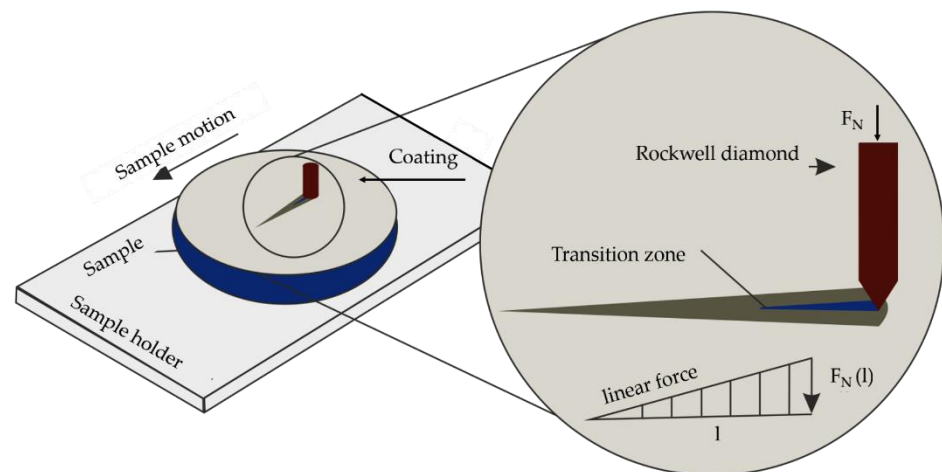


Figure 5. Scratch test schematic diagram.

The instrumental hardness, Young's modulus, and the maximum indentation depth of the tested materials were measured using an ultra nano hardness tester (UNHT) from Anton Paar. A Berkovich diamond indenter with an opening angle of 142.5° and a rounding radius of ~ 100 nm was used for the measurement. During the test, the samples were loaded with a force of 10 mN. Then, the indenter remained under load for 5 s, after which the sample was loaded. The results are presented in Section 3.1.

The thickness of the deposited carbon layers was examined by microscopic observations of cross-sections using a Phenom XL scanning electron microscope equipped with an EDS energy dispersion spectrometer. An accelerating voltage of 15 kV and a magnification of $\times 24,000$ were used. The study was supplemented by linear elemental distributions. The results of the experiments are presented in Section 3.2.

An optical tensiometer Attension theta flex was used to determine wettability and surface tension. Wettability was evaluated on the basis of the interaction of the studied surfaces with aqueous solutions. High wettability–hydrophilicity occurs at a contact angle (θ) of less than 90° and low wettability–hydrophobicity occurs at a contact angle (θ) of more than 90° (Figure 6).

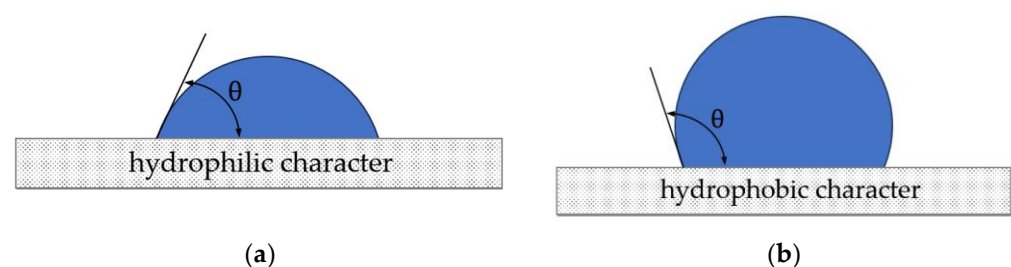


Figure 6. Wettability of the surface of a solid: (a) good wettability (hydrophilicity) and (b) hydrophobicity.

A droplet of the measuring liquid is most often spherical in shape, and the contact angle is formed between the surface of the solid and the tangent to the droplet surface drawn from the contact point of the three phases: solid–liquid–air. The most popular technique for measuring the contact angle to determine the wettability is the sessile drop method. The test consists of placing a drop of demineralized water with a volume of 4 μL on the sample surface and measuring it immediately. The average values of contact angles were determined based on five measurement series.

Additionally, the use of One Attention software (version 4.0.4) allowed determining the surface tension by the Owens–Wendt method. The appropriate choice of measuring liquids is crucial. One of them should be characterized by a low value of the polar component and a high value of the dispersive component (e.g., diiodomethane), while the other measuring liquid should be characterized by a high value of the polar component and a low value of the dispersive component (e.g., demineralized water) [47]. The tests were performed at a temperature of $23\text{ }^{\circ}\text{C} \pm 1$ and a humidity of $55\% \pm 5$. The results of the contact angle and surface tension tests are presented in Section 3.3.

Observations of the geometric structure of coating surfaces before and after tribological tests were performed using a confocal microscope with Leica DCM8 interferometric mode. Surface topography was evaluated on the basis of axonometric (3D) images, surface profiles, and amplitude parameters. A $250 \times 350\text{ }\mu\text{m}$ area was analyzed, and the results are presented in Section 3.4.

Tribological tests were carried out using an Anton Paar TRB³ tribometer in reciprocating motion in dry friction conditions and under lubricated friction with 10% BeCool Met 3920 coolant (Table 2).

Table 2. Physicochemical properties of the coolant.

Parameter	Value
Color	light yellow
pH (10 g/L) at 20 $^{\circ}\text{C}$	9.5
Flash point	>100 $^{\circ}\text{C}$
Density at 20 $^{\circ}\text{C}$	1.01 g/cm ³
Water solubility/miscibility	emulsifiable

During tribological tests, a loading force of 10 N, 10,000 cycles, and an amplitude of 1 Hz were applied. The counter sample was an Al_2O_3 ball with a diameter of 6 mm and R_a equal to 0.32 μm . A photograph of the friction node is shown in Figure 7.

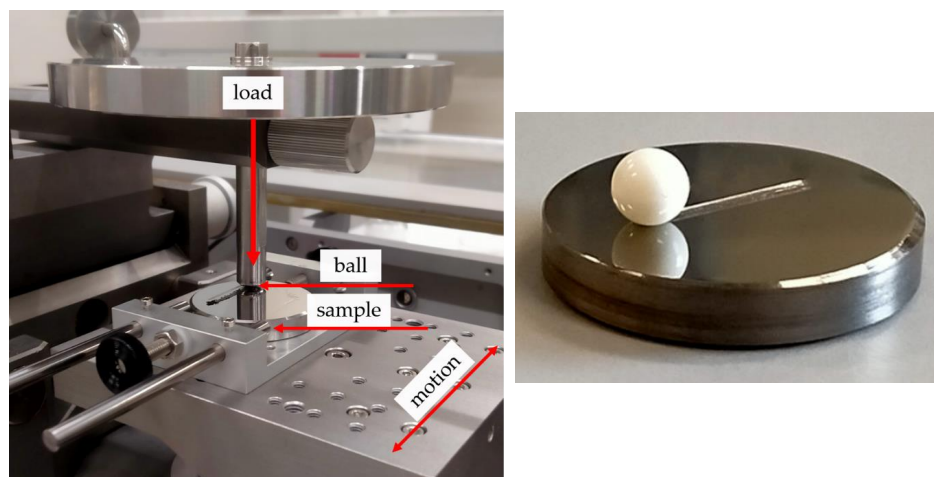


Figure 7. Friction pair, tribological test.

The tests were repeated three times for each sliding pair at the set parameters, and the average values of friction coefficients and linear wear were determined (Section 3.5).

After the tests, the samples and counter samples were subjected to microscopic observations to find the most important wear indicators, i.e., abrasion maximum depth and volume. In addition, amplitude parameters in the wear traces were determined in a $150 \times 200 \mu\text{m}$ area.

The tests were complemented by chemical composition analyses in micro-areas. Section 3.7 describes the structures and elemental distribution on the surface.

3. Results

3.1. Adhesion and Hardness

Figure 8 shows the results of the scratch test of a-C:H:Si coatings deposited on the polished (a) and sandblasted (b) surfaces. The diagrams show optical images of the scratches as well as plots of friction coefficients— μ , loading force (F_n), acoustic emission (Ae)—and the values of critical forces (LC₁–LC₅).

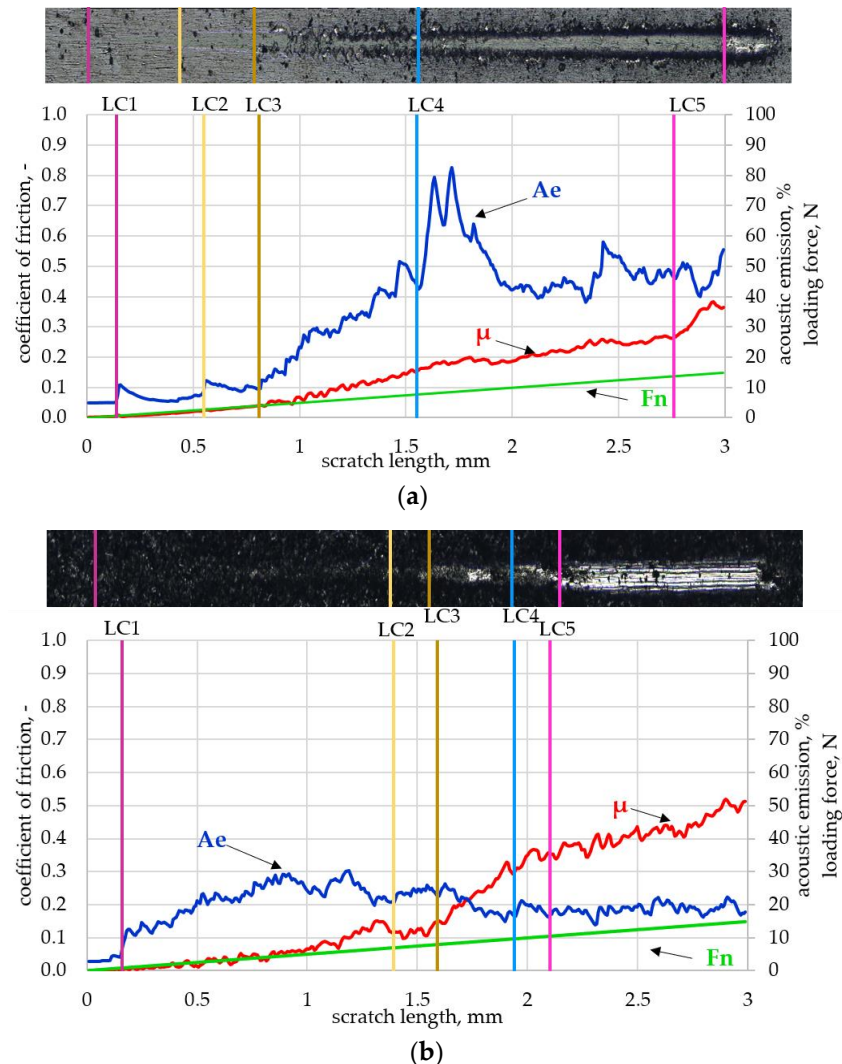


Figure 8. Results of the a-C:H:Si scratch tests: (a) polished surface and (b) sandblasted surface.

The results of the scratch test of the a-C:H coating deposited on the polished surface indicated its good adhesion to the Ti13Nb13Zr substrate. Although characteristic peaks were observed on the acoustic emission plot and cracks and pitting were observed on the optical image, ultimately, the coating remained unbroken. On the sandblasted sample

under an F_N load of about 10.5 N, the applied carbon layer delaminated. The tests indicated a relationship between roughness and adhesion to the metallic substrate. The coating deposited on the less-textured sample had better adhesion than the layer applied to the sandblasted surface.

Table 3 shows the average values of essential mechanical parameters: instrumental hardness (H_{IT}), Young’s modulus (E_{IT}), and maximum indenter penetration depth (hm) calculated based on five measurement series.

Table 3. Hardness measurement results.

Sample	Parameter and Unit						
	Instrumental Hardness (H_{IT}), MPa		Young’s Modulus (E_{IT}), GPa		Maximum Penetration Depth (h_m), nm		
	Mean	std. dev	Mean	std. dev	Mean	std. dev	
Ti13Nb13Zr	3841	16.1	104.2	0.4	350	11	
a-C:H:Si	polished	22,191	732.5	179.2	5.8	177	3
	sandblasted	18,572	357.8	129.8	7.2	206	15

Mechanical tests showed changes in Ti13Nb13Zr alloy hardness and Young’s modulus due to the deposition of diamond-like coatings. Both parameters increased by almost 82% and 42%, respectively. The indenter penetration depth (hm) was closely related to HIT and EIT values. The sample with the diamond-like coating produced the smallest indentation, 177 nm. The tribological characteristics of the analyzed materials, including wear resistance, were expected to be directly impacted by the increase in hardness.

3.2. Coating Thickness

Figure 9 shows a cross-sectional image of the a-C:H:Si coating microstructure along with the linear distribution of elements. The thickness of the coating was determined from observations in three areas.

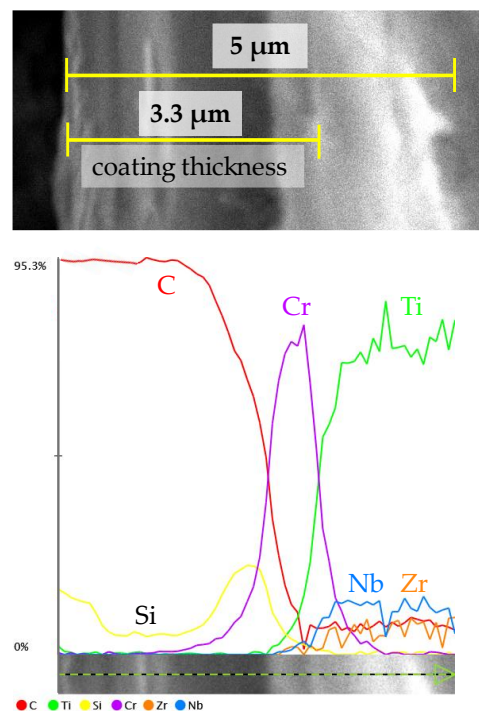


Figure 9. Linear distribution of elements on the cross-section, and the coating thickness.

Linear analysis of the elemental distribution in the diamond-like coating showed that the near-surface layer consisted of carbon and silicon. At a depth of about 2.6 μm from the surface, the interlayer of chromium was observed. Its function was to ensure adequate coating-to-metallic substrate adhesion. The analysis also indicated the presence of titanium, niobium, and zirconium (elements derived from the substrate).

3.3. Contact Angle and Surface Tension

The wettability of the surface and the energy of the materials play an important role during the operation of tribological systems. Figures 10 and 11 show example photos of demineralized water droplets deposited on carbon coatings. In turn, Tables 4 and 5 summarize the average results of the recorded contact angles and surface tension.

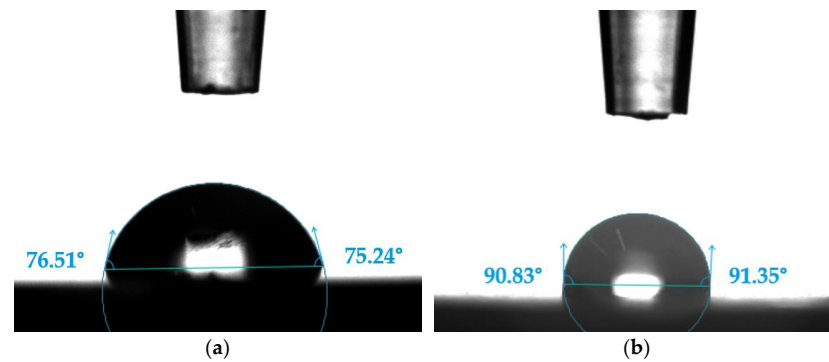


Figure 10. Examples of photographs showing demineralized water droplets on Ti13Nb13Zr: (a) polished and (b) sandblasted.

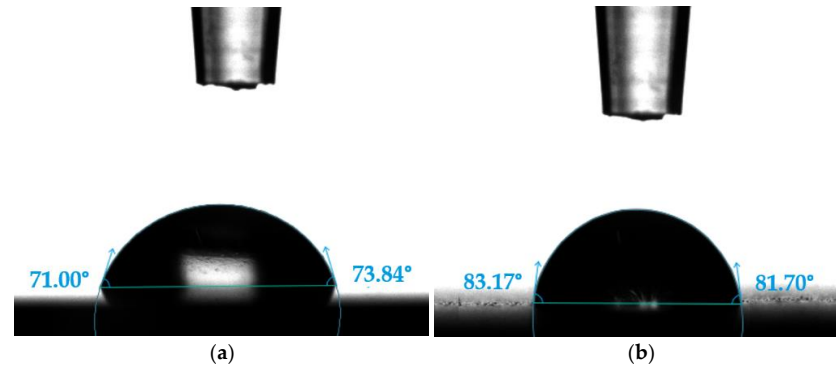


Figure 11. Examples of photographs showing demineralized water droplets on a-C:H:Si: (a) polished and (b) sandblasted.

Table 4. Contact angle.

Number	Ti13Nb13Zr		a-C:H:Si	
	Polished	Sandblasted	Polished	Sandblasted
	contact angle, °			
1	77.79	90.83	72.63	83.29
2	75.17	89.34	72.46	82.44
3	77.40	90.65	74.38	84.12
4	75.58	91.78	73.21	84.28
5	76.68	89.98	72.19	82.91
mean	76.52	91.12	72.97	83.40
std. dev.	1.01	0.84	0.77	0.70

Table 5. Surface tension.

Number	Ti13Nb13Zr		a-C:H:Si	
	Polished	Sandblasted	Polished	Sandblasted
surface tension, mN/m				
1	43.82	35.33	40.25	35.05
2	41.71	35.22	43.40	34.98
3	42.42	34.54	40.64	35.35
4	40.86	35.91	42.30	36.30
5	43.35	34.26	42.82	37.22
mean	42.43	35.05	41.88	35.78
std. dev.	1.07	0.58	1.22	0.86

The results presented above indicate that surface topography affected the values of contact angles and surface tension. Although both samples tested showed hydrophilic character, the carbon coating deposited on the polished surface had about 13% lower contact angles than the coating deposited on the sandblasted surface. The value of surface tension decreased with increasing surface roughness.

3.4. Confocal Microscopy Results

Surface topography analyses performed before tribological tests were based on 3D axonometric images, primary profiles, and amplitude parameters (Sa, arithmetic mean of the surface roughness deviation; Sp, maximum peak height; Sv, maximum indentation depth; Sku, surface peakness (kurtosis); Ssk, degree of symmetry (skewness)). The data presented in Figures 12 and 13 and Table 6 are a valuable source of information on the performance characteristics of the tested surfaces.

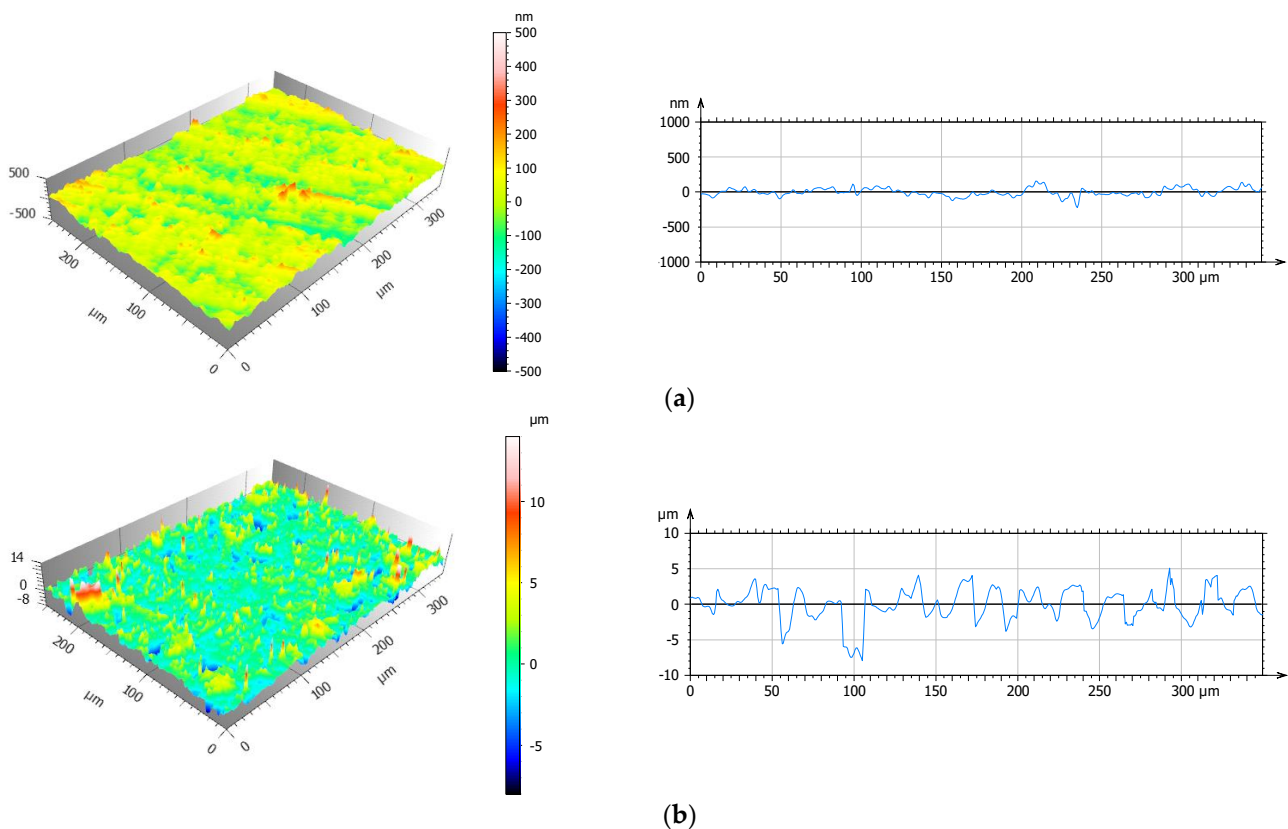


Figure 12. Three-dimensional axonometric images and primary profiles of Ti13Nb13Zr: (a) polished and (b) sandblasted.

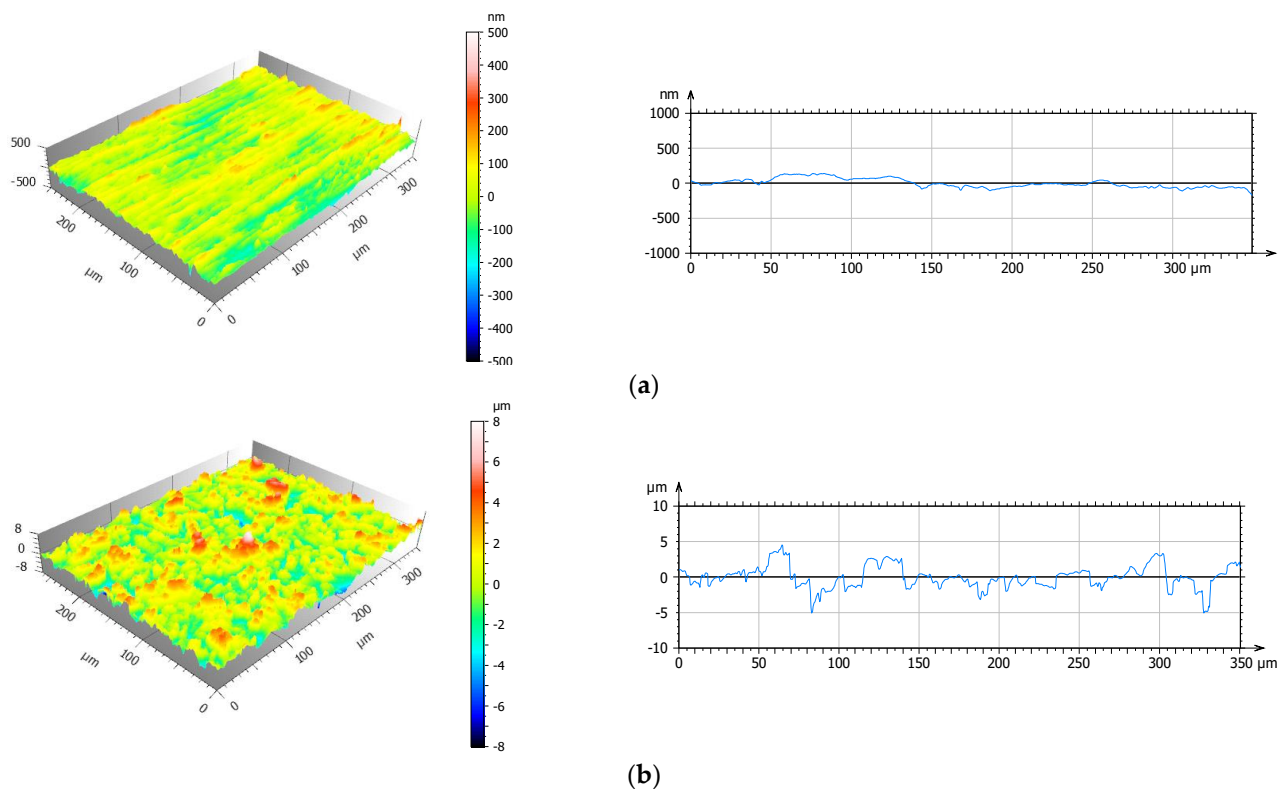


Figure 13. Three-dimensional axonometric images and primary profiles of a-C:H:Si coatings deposited on surfaces: (a) polished and (b) sandblasted.

Table 6. Amplitude parameters of Ti13Nb13Zr and coatings before tribology testing.

	Ti13Nb13Zr		a-C:H:Si	
	Polished	Sandblasted	Polished	Sandblasted
Sa, μm	0.05	1.51	0.05	1.34
Sv, μm	0.34	8.63	0.33	7.11
Sp, μm	0.32	14.8	0.30	7.28
Ssk	0.15	0.26	0.17	0.06
Sku	3.67	6.72	4.32	3.77

The results of the geometric structure of the surface indicated that the deposition of a diamond-like coating doped with silicon significantly affected the change in the roughness parameters of Ti13Nb13Zr titanium alloy, with the greatest differences observed for the sandblasted surface (Sv decreased by about 17% and Sp by 51%). Analysis of the results in Table 6 showed that the polished a-C:H:Si had the lowest roughness, while sandblasted Ti13Nb13Zr had the highest. This indicated that the sandblasted surface had the highest peaks and deepest valleys of all the samples analyzed. Information on the nature of surface topography is also provided by skewness (Ssk) and kurtosis (Sku). The results indicated that the highest skewness of 0.26 was obtained for the sandblasted Ti13Nb13Zr surface, which indicated the presence of steep peaks with sharp tips on the surface of this sample. A 35% decrease in Ssk as a result of DLC coating deposition demonstrated the loss of peakness. A kurtosis value of three meant that the distribution of peaks and valleys on the surface was uniform and close to a normal distribution. This was the distribution we dealt with in the case of the polished Ti13Nb13Zr surface. A significant increase in Sku—up to 6.72 in the case of the Ti13Nb13Zr sandblasted sample—indicated that, as a result of the physical and chemical treatments applied, surface topography changed (an increase in the peaks and valleys on the Ti13Nb13Zr alloy). The topography of friction pair

surfaces affected the value of the friction coefficient and wear rate. An accurate analysis of the geometric structure of the surface allowed a preliminary prediction of tribological properties already at the stage of surface layer formation.

3.5. Tribological Tests

The tribological properties of materials are critical for the proper operation of components. The purpose of this research was to determine tribological characteristics (coefficients of friction and linear wear) of the friction pairs studied. Figure 14 shows diagrams of average values of friction coefficients (a) and linear wear (b) for all the materials tested under dry friction and friction lubricated with BeCool Met 3920 coolant.

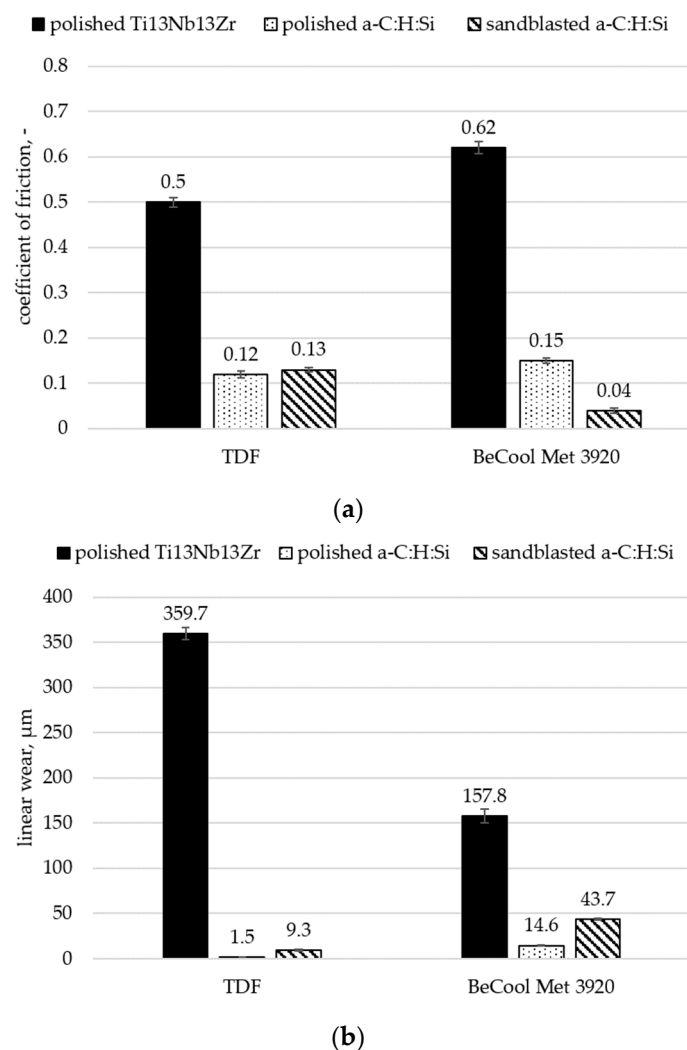


Figure 14. Average values of friction coefficients (a) and linear wear (b).

The results of the tribological tests indicated that the titanium alloy had the highest coefficients of friction and linear wear of all tested samples. Moreover, it was observed that the application of the lubricant simultaneously contributed to increasing the friction coefficient of the Ti13Nb13Zr- Al_2O_3 friction pair by about 20% and reducing its linear wear by more than 50%. Compared with the sandblasted sample, the a-C:H:Si coating deposited on the polished surface had lower coefficients of friction and linear wear under dry friction by about 10% and 83%, respectively. In contrast, due to the presence of depressions and elevations, the a-C:H:Si coating applied to the sandblasted sample was characterized by a longer run-in time and better lubrication of the friction node. This was evidenced by the recorded values of friction coefficients and linear wear during lubricated friction with

BeCool Met 3920 coolant. Their values were 75% lower and 65% higher, respectively, compared with polished a-C:H:Si.

3.6. Assessment of Surface Geometric Structure of Samples and Counter Samples

After tribological tests, both the samples (Figures 15 and 16) were subjected to microscopic observations. Optical and 3D axonometric images, abrasion profiles, and the maximum abrasion depth on the cross-section are presented in Figure 17. The counter samples (Figures 18 and 19) were also tested. The values of amplitude parameters are summarized in Tables 7 and 8. Tables 9 and 10 show the most important indicator of friction pair surface wear: the volume of abrasion.

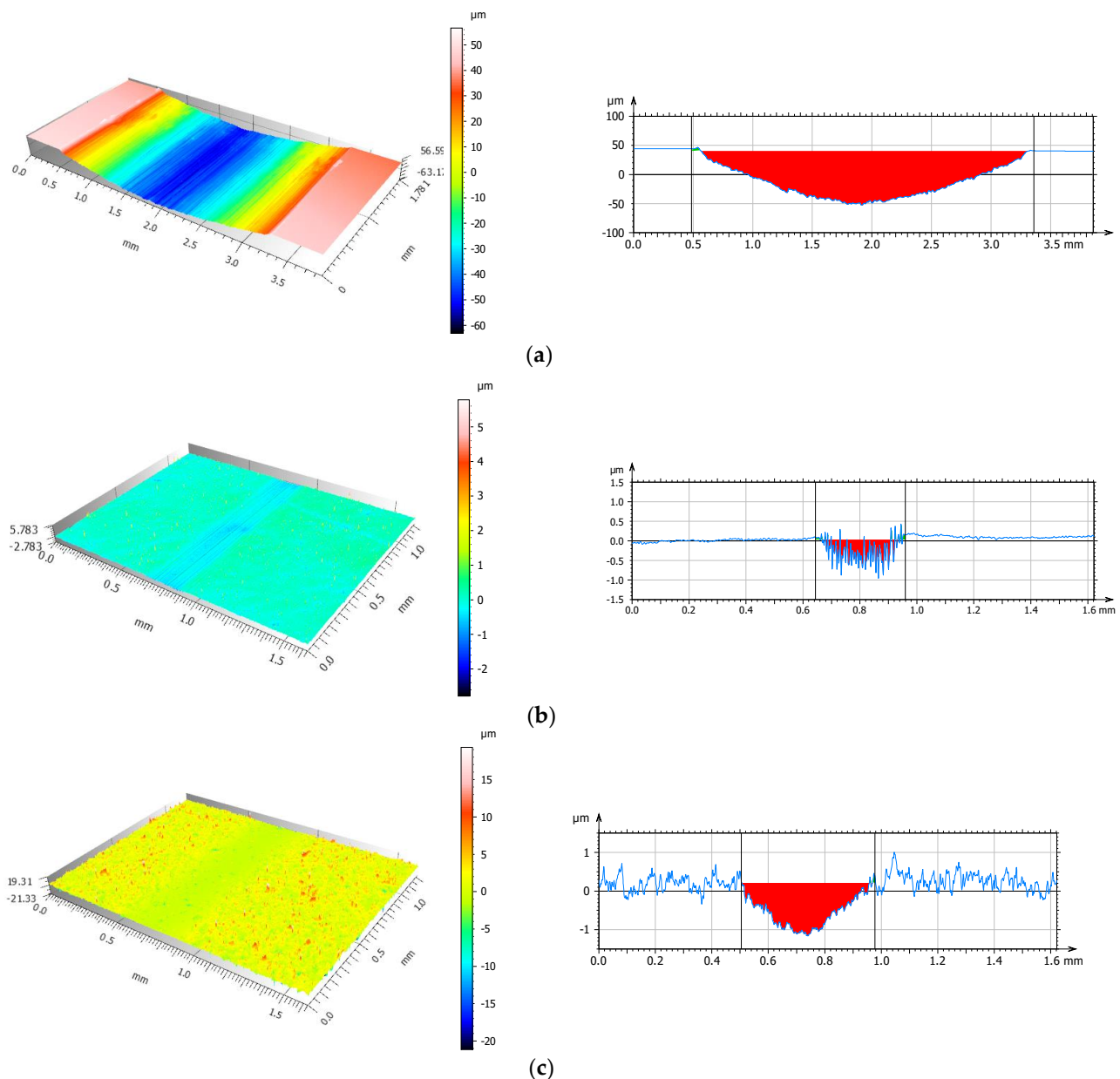


Figure 15. Three-dimensional axonometric images and average values of abrasion profiles after friction in dry conditions: (a) polished Ti13Nb13Zr sample, (b) polished a-C:H:Si coating, and (c) sandblasted a-C:H:Si coating.

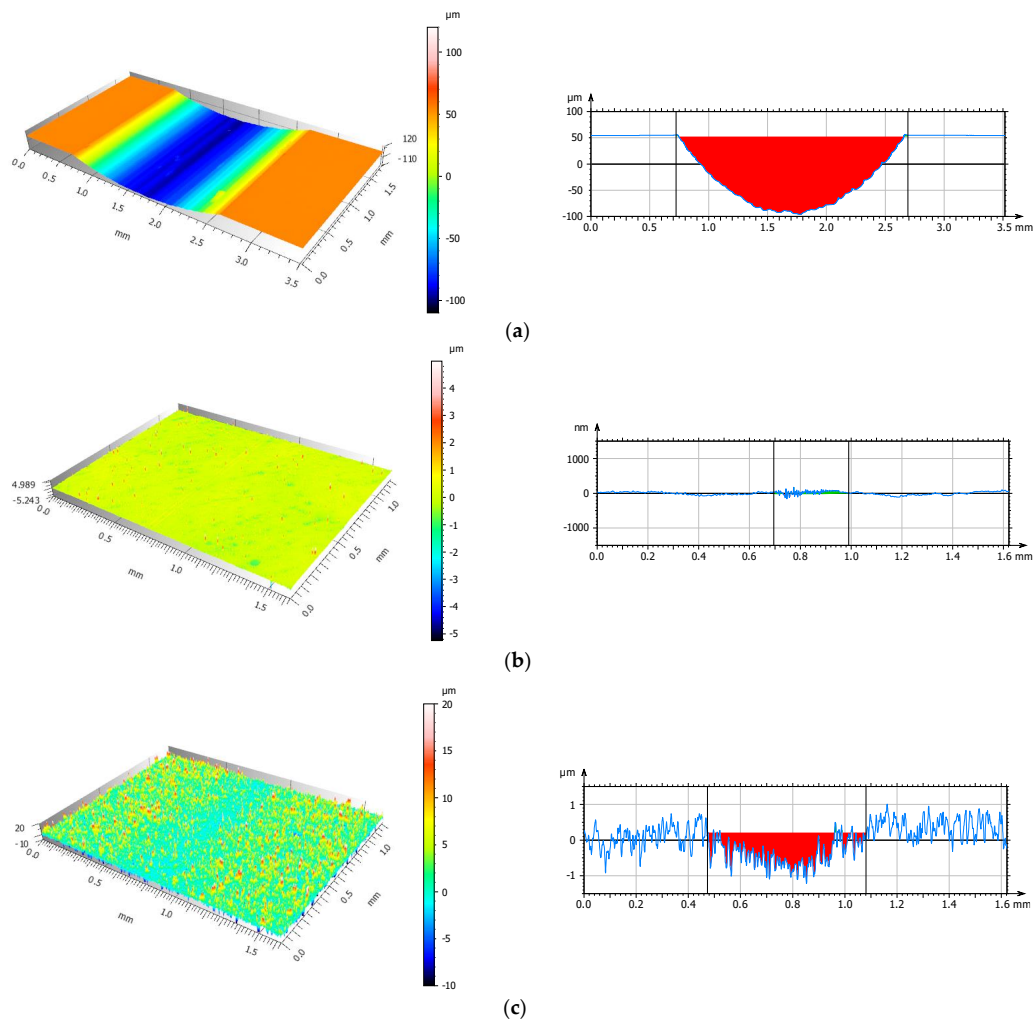


Figure 16. Three-dimensional axonometric images and average values of abrasion profiles after lubricated friction with BeCool Met 3920: (a) polished Ti13Nb13Zr sample, (b) polished a-C:H:Si coating, and (c) sandblasted a-C:H:Si coating.

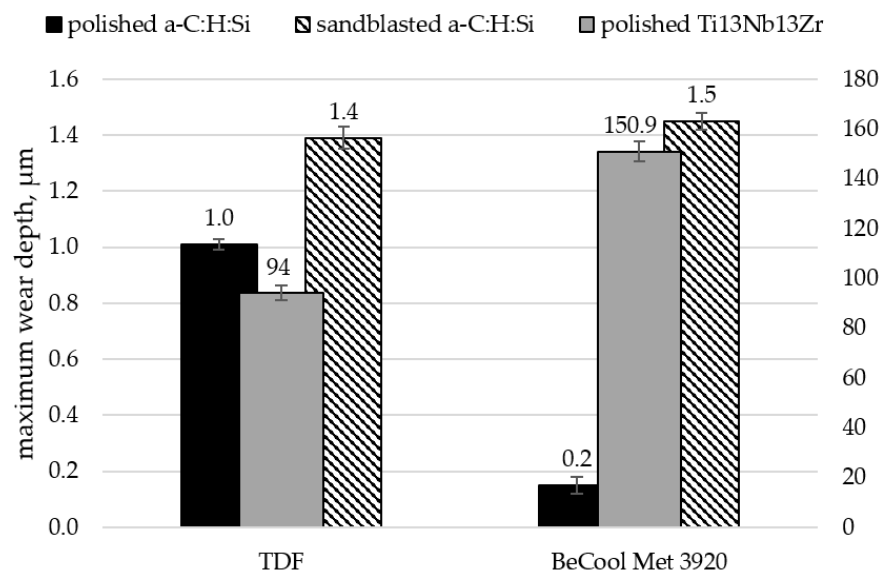


Figure 17. Maximum depth of wear trace on a cross-section.

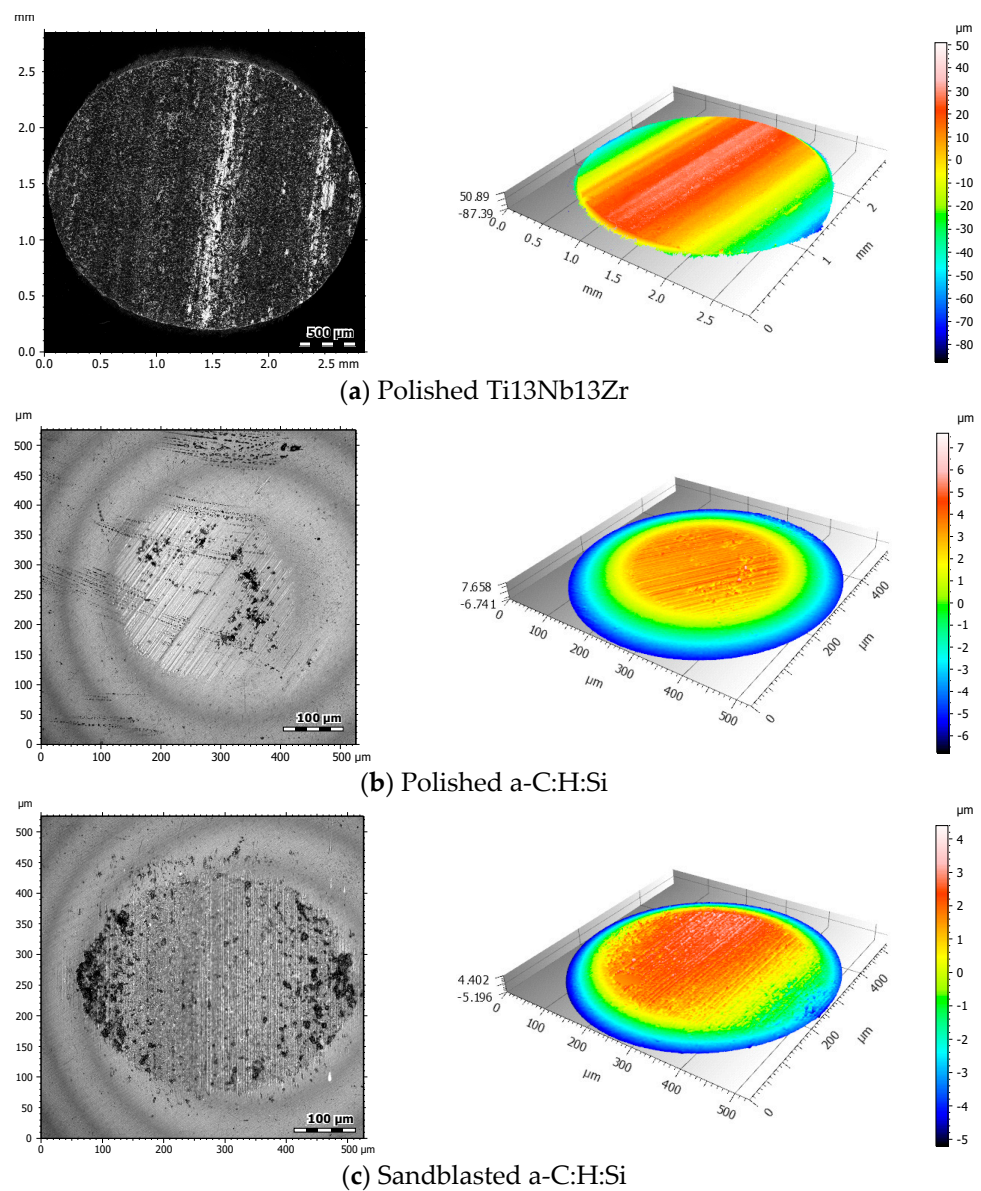


Figure 18. Optical and 3D axonometric wear images of balls after dry friction (a) Polished Ti13Nb13Zr; (b) Polished a-C:H:Si; (c) Sandblasted a-C:H:Si.

Table 7. Amplitude parameters of the Ti13Nb13Zr alloy and coatings after friction in dry conditions.

	Ti13Nb13Zr		a-C:H:Si	
	Polished	Sandblasted	Polished	Sandblasted
Sa, μm	1.13	not measured	0.24	0.18
Sv, μm	3.92	not measured	1.01	10.13
Sp, μm	5.89	not measured	0.97	4.59
Ssk	−0.56	not measured	−0.26	−4.89
Sku	2.77	not measured	2.57	34.62

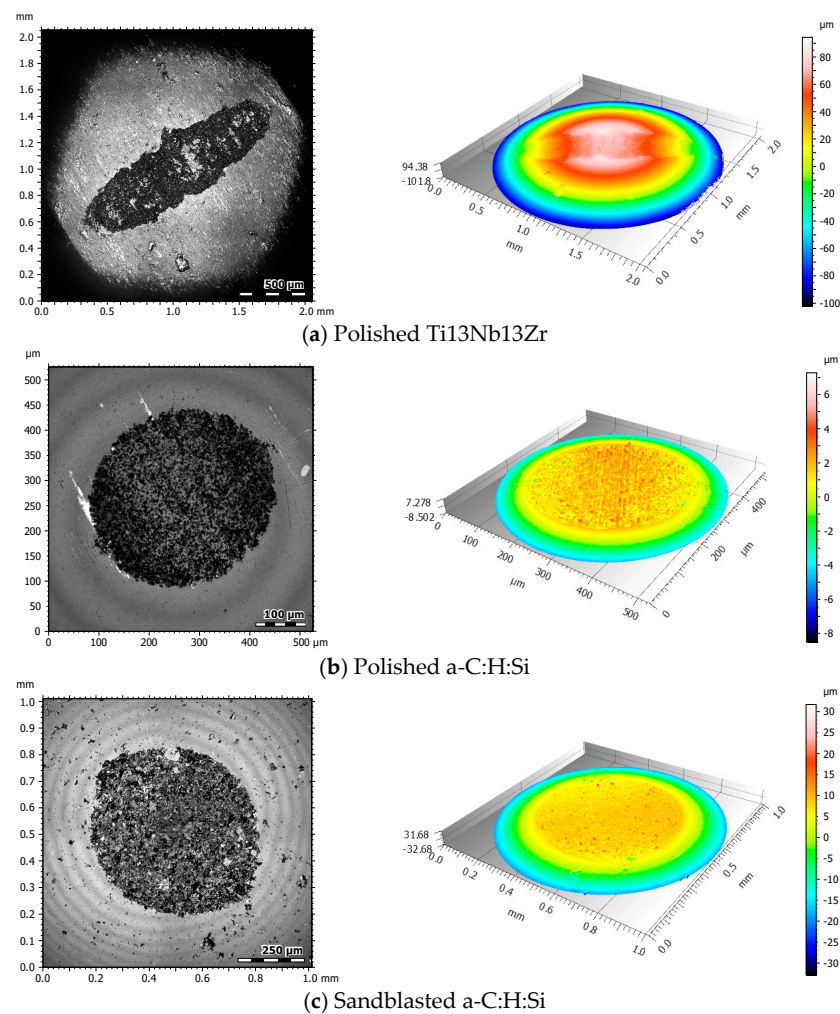


Figure 19. Optical and 3D axonometric wear images of balls after lubricated friction with BeCool Met 3920.

Table 8. Amplitude parameters of the disc surface geometric structure after lubricated friction with BeCool Met 3920.

	Ti13Nb13Zr		a-C:H:Si	
	Polished	Sandblasted	Polished	Sandblasted
Sa, μm	4.78	not measured	0.15	1.2
Sv, μm	10.22	not measured	0.98	32.92
Sp, μm	14.16	not measured	3.83	26.80
Ssk	0.43	not measured	2.25	−1.32
Sku	2.38	not measured	27.05	80.45

Table 9. Wear volume.

	Wear Volume, μm ³	
	TDF	BeCool Met 3920
polished Ti13Nb13Zr	260 × 10 ⁶	327 × 10 ⁶
sandblasted Ti13Nb13Zr	not measured	not measured
polished a-C:H:Si	75 × 10 ³	31 × 10 ³
sandblasted a-C:H:Si	552 × 10 ³	789 × 10 ³

Table 10. Ball wear volume.

	Wear Volume, μm^3	
	TDF	BeCool Met 3920
polished Ti13Nb13Zr	211×10^6	54×10^6
sandblasted Ti13Nb13Zr	not measured	not measured
polished a-C:H:Si	35×10^3	84×10^3
sandblasted a-C:H:Si	222×10^3	546×10^3

The results of microscopic observations after tribological tests indicated that the values of amplitude parameters changed depending on the analyzed surface and friction conditions. These changes were indicative of a decrease or increase in the wear trace roughness. The greatest heights and valleys were observed in the sandblasted sample with the a-C:H:Si coating in dry conditions and with BeCool Met 3920 coolant lubrication. Analysis of 3D axonometric images found that the dominant wear mechanism on Ti13Nb13Zr was tribochemical wear through oxidation and abrasive wear with plowing effect and microcutting. The strong affinity of titanium for oxygen caused the formation of a thin passive layer composed of TiO_2 on the surface of the Ti13Nb13Zr alloy. As a result of friction, this layer cracked and crumbled, leading to intensive wear. Additionally, this process was intensified by the presence of loose wear products in the friction contact. Different wear mechanisms occurred during friction with the coatings. Abrasive wear by scratching and microcutting predominated, and asperities on the coating deposited on the sandblasted surface were sheared.

The results of the wear trace depth test showed that carbon coatings deposited on Ti13Nb13Zr were characterized by high wear resistance, with the best efficiency achieved on the polished surface. The lowest values were recorded for the polished surface under dry and lubricated friction with BeCool Met 3920. In the case of the coating deposited on the sandblasted specimen, the results from both friction conditions were comparable. Comparison of the values of the maximum wear depths to the coating thickness (Section 3.2) found that the deposited layers performed very well in terms of their functional characteristics throughout the tribological tests. None of the layers was fully consumed.

The results of the wear trace and volume tests supported the conclusion about the low wear resistance of the titanium alloy and were consistent with the results reported in Section 3.5. The coating deposited on the polished surface had the highest wear resistance, with the best antiwear efficiency obtained with BeCool Met 3920 lubrication. This indicated that this surface interacted well with the proposed lubricant. Compared with the a-C:H:Si on the polished surface, the wear of the a-C:H:Si coating deposited on the sandblasted surface was higher under dry and lubricated friction by 85 and 96%, respectively.

The highest wear of the counter samples (balls) was recorded for the interaction with the Ti13Nb13Zr alloy. In addition, it was observed that the use of a lubricant reduced the ball wear by about 75%. In the case of a-C:H:Si- Al_2O_3 friction junctions, the volume of counter sample wear increased as a result of the application of BeCool Met 3920 by about 41% for the polished surface and 60% for the sandblasted sample.

3.7. EDS Analysis of the Wear Trace after Tribological Tests

Due to limitations resulting from the too small measuring area of the scanning microscope and the inability to present the entire wear trace, Figures 20–25 show maps of elemental distribution from part of the wear trace and the frictionless surface. The aim was to demonstrate differences in the distribution of individual elements on surfaces with and without friction.

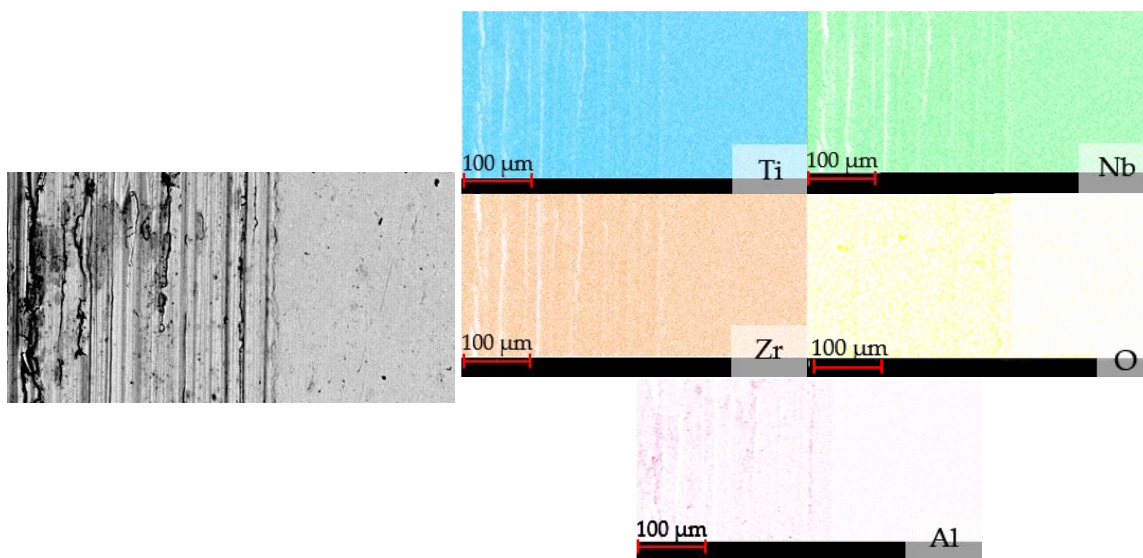


Figure 20. SEM image and elemental distribution on the surface of the Ti13Nb13Zr after dry friction.

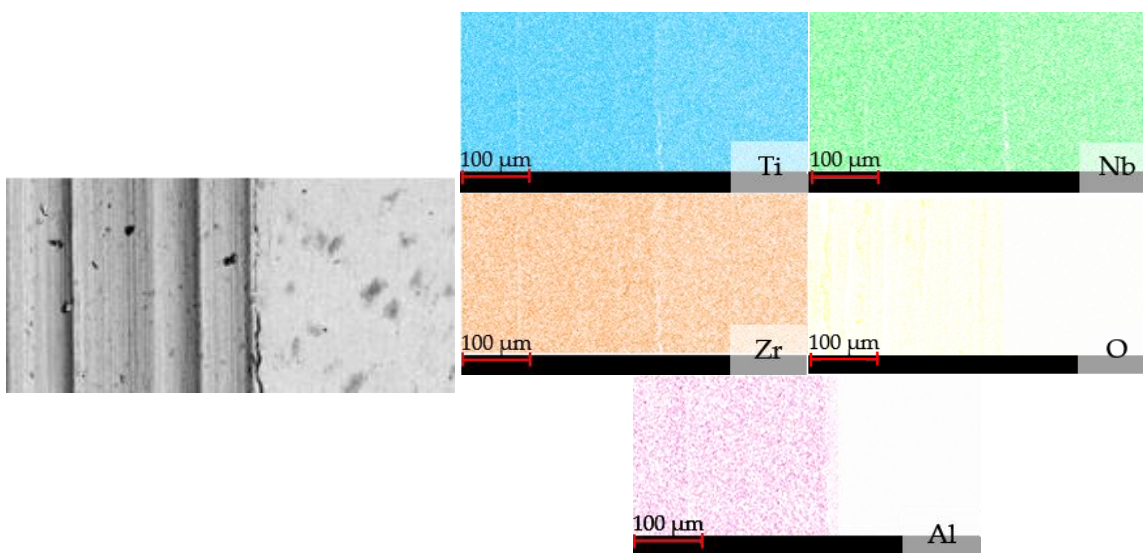


Figure 21. SEM image and elemental distribution on the surface of the Ti13Nb13Zr after friction with BeCool Met lubrication.

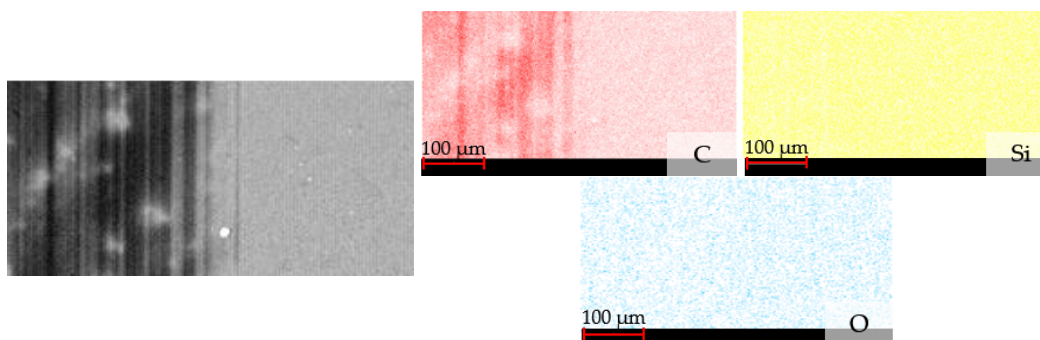


Figure 22. SEM image and elemental distribution on the surface of the polished a-C:H:Si coating after dry friction.

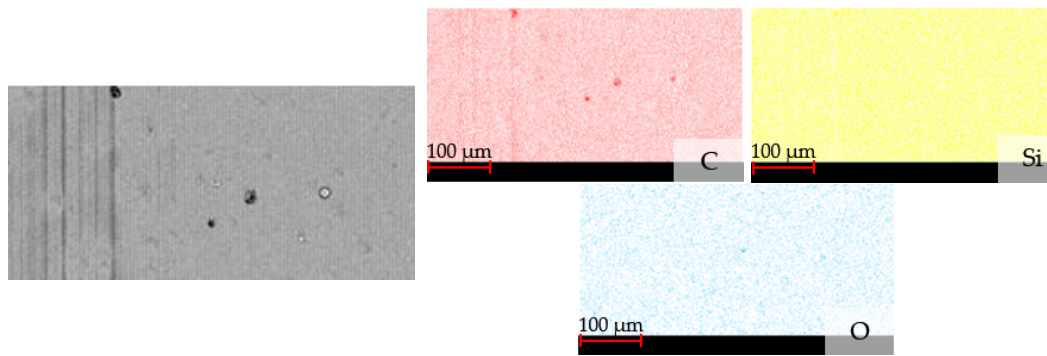


Figure 23. SEM image and elemental distribution on the surface of the polished a-C:H:Si coating after friction with BeCool Met lubrication.

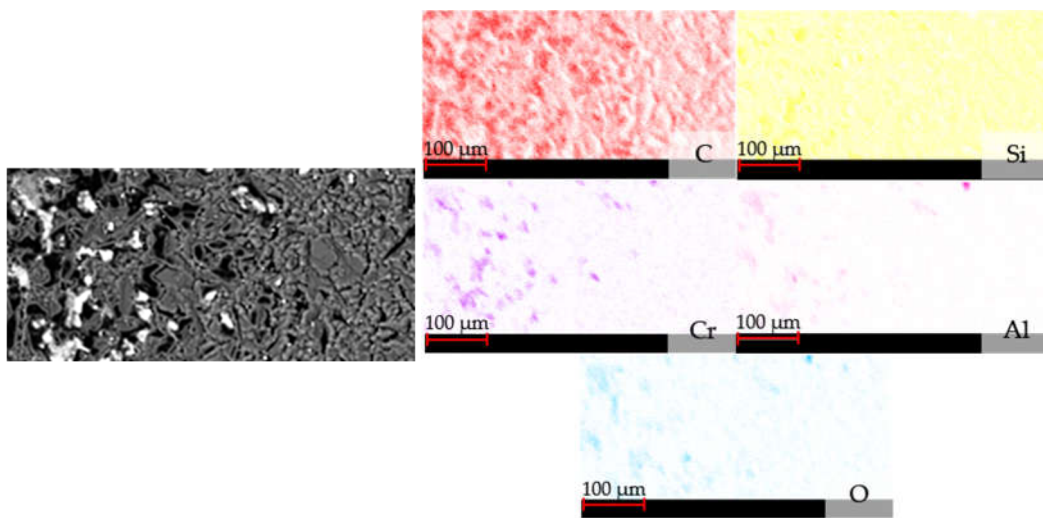


Figure 24. SEM image and elemental distribution on the surface of the sandblasted a-C:H:Si coating after dry friction.

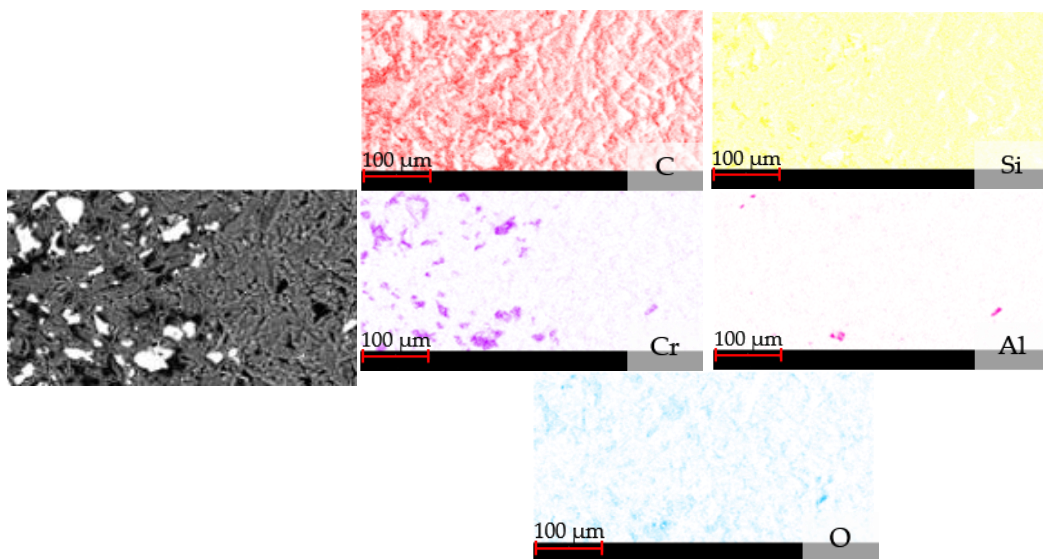


Figure 25. SEM image and elemental distribution on the surface of the sandblasted a-C:H:Si coating after friction with BeCool Met lubrication.

The maps of the wear trace elemental distribution for Ti13Nb13Zr alloy after dry friction revealed the highest concentration of titanium and its even distribution over the

entire area. In the case of niobium and zirconium, similar density and color intensity were observed, which indicated a similar percentage of these elements in the Ti13Nb13Zr alloy. Analysis in the friction area indicated the presence of oxygen and aluminum with a much lower degree of color saturation than in the case of titanium, niobium, and zirconium. Higher concentrations of these elements were found inside the abrasion trace than outside of it. The presence of aluminum resulted from the transfer of the counter sample material (the Al₂O₃ ball). A similar concentration of these elements was observed in the wear traces of the Ti13Nb13Zr alloy after friction with BeCool Met 3920 lubrication. In the case of a-C:H:Si coatings deposited on a polished surface, carbon and silicon dominated. A small concentration of oxygen was also observed both inside and outside the wear trace, and no aluminum was detected. EDS analysis of coatings applied to sandblasted surfaces indicated the highest percentages of carbon and silicon. Additionally, the chrome interlayer was exposed due to friction. Aluminum from the counter sample and oxygen were also detected in the abrasion traces, indicating surface oxidation of the sandblasted coating as a result of friction.

4. Conclusions

The following conclusions were formulated based on the test results:

1. The coatings of about 3 μm produced using the CVD technique had homogeneous structures without defects in the form of voids or delamination. The linear distribution of elements confirmed the presence of all elements assumed in the fabrication process.
2. The application of physicochemical treatments, polishing and sandblasting, as well as the deposition of the DLC coatings, changed the stereometric parameters of the Ti13Nb13Zr alloy surface, thereby altering the results of measured surface energy, obtained adhesion strength, and tribological properties.
3. The topography of the surface layer affected the measurements of contact angles and surface tension. Coatings deposited on sandblasted surfaces had higher contact angles and lower surface tension with respect to the polished a-C:H:Si by about 15%.
4. Adhesion test results showed that the coating-to-substrate adhesion of the a-C:H:Si coating deposited on the polished surface was better than on the sandblasted sample.
5. The deposition of diamond-like coatings doped with silicon contributed to the increase in the hardness of the Ti13Nb13Zr alloy by approximately 82%. The improvement of mechanical parameters had a direct impact on the increase in the resistance to tribological wear of this material.
6. The results of tribological tests and microscopic observations of the samples showed that the Ti13Nb13Zr alloy had the highest friction coefficients and wear among all the samples tested, amounting to 0.05 and 359.7 μm, respectively, in dry friction conditions, and 0.62 and 157.8 μm in lubricated friction with BeCool Met 3920. As for coatings, the best characteristics were obtained for the polished surface, for which the lowest friction coefficients and volumetric wear were recorded. Under dry friction, the volumetric was approximately 85% lower, while, with lubrication, it was approximately 95% lower compared with the sandblasted sample.
7. The applied lubricant in the form of a coolant interacted synergistically with the a-C:H:Si coating surface, both polished and sandblasted. The reduction in friction coefficients of the coating applied to the sandblasted sample was more significant (about 75%) compared with the polished sample without coating, and ensured stable operation during the tests.
8. The dominant wear mechanism in the case of the Ti13Nb13Zr titanium alloy was tribochemical wear through oxidation and abrasive wear with plowing and micro-cutting. Additionally, these processes were intensified by the presence of loose wear products in the friction zone. However, in the case of diamond-like coatings, abrasive wear by scratching and microcutting dominated.
9. The maps of the wear trace elemental distribution for Ti13Nb13Zr alloy after dry friction and friction with BeCool Met lubrication revealed the highest concentration of

titanium. In the case of niobium and zirconium, the percentages of these elements in the Ti₁₃Nb₁₃Zr alloy were similar. Higher concentrations of oxygen and aluminum were found inside the abrasion trace than outside of it. The presence of aluminum resulted from the transfer of the counter sample material. In the case of a-C:H:Si coatings, carbon and silicon dominated. Additionally, in the case of a-C:H:Si coatings deposited on the sandblasted surface, a chrome interlayer was exposed due to friction. Aluminum from the counter sample and oxygen were also in the abrasion traces, indicating surface oxidation of the sandblasted coating as a result of friction.

10. The application of diamond-like coatings on Ti₁₃Nb₁₃Zr titanium alloy improved the functional properties of unlubricated and coolant-lubricated friction nodes.

Author Contributions: Conceptualization: K.P., M.M., J.K. and K.R.-K.; methodology: K.P. and M.M.; writing—original draft preparation: K.P. and J.K.; writing—review and editing: K.P., M.M., J.K. and K.R.-K.; supervision, M.M. All authors have read and agreed to the published version of the manuscript.

Funding: This research received no external funding.

Institutional Review Board Statement: Not applicable.

Informed Consent Statement: Not applicable.

Data Availability Statement: Not applicable.

Conflicts of Interest: The authors declare no conflict of interest.

References

1. Ehiasarian, A.; Purandare, Y.; Sugumaran, A.; Hovsepian, P.; Hatto, P.; De Backer, J. Improving the Quality of Friction Stir Welds in Aluminium Alloys. *Coatings* **2021**, *11*, 539. [[CrossRef](#)]
2. Dobrzański, L.A.; Dobrzańska-Danikiewicz, A.D. Obróbka powierzchni materiałów inżynierskich. *Open Access Libr.* **2011**, *5*, 1–480.
3. Burakowski, T.; Wierzchoń, T. *Inżynieria Powierzchni Metali*. Wydawnictwo Naukowo-Techniczne: Warsaw, Poland, 1995.
4. Niemczewska-Wójcik, M. *Dualny System Charakteryzowania Powierzchni Technologicznej i Eksploatacyjnej Warstwy Wierzchniej Elementów Trących*; Wydawnictwo Naukowe Instytutu Technologii Eksploatacji PIB: Radom, Poland, 2018.
5. Zaleski, K.; Matuszak, J.; Zaleski, R. *Metrologia Warstwy Wierzchniej*. Wydawnictwo Politechniki Lubelskiej: Lublin, Poland, 2018.
6. Legutko, S.; Nosal, S. *Kształtowanie Technologicznej i Eksploatacyjnej Warstwy Wierzchniej Części Maszyn*; OWN PAN: Poznań, Poland, 2004.
7. Posmyk, A. *Kształtowanie Właściwości Tribologicznych Warstw Wierzchnich Tworzyw na Bazie Aluminium*; Wydawnictwo Politechniki Śląskiej: Gliwice, Poland, 2001.
8. Senatorski, J. *Podnoszenie Tribologicznych Właściwości Materiałów Przez Obróbkę Ciepłą i Powierzchniową*; Wydawnictwo Instytut Mechaniki Precyzyjnej: Warsaw, Poland, 2003.
9. Styp-Rekowski, M.; Musiał, J. Wear processes accompanying rolling friction. *Probl. Eksploat.* **2006**, *3*, 189–199.
10. Gałda, L. Wybrane czynniki wpływające na odporność na zużycie węzłów ślizgowych. *Autobusy* **2016**, *6*, 861–865.
11. Płaza, S.; Margielewski, L.; Celichowski, G. *Wstęp do Tribologii i Tribochemia*; Wydawnictwo Uniwersytetu Łódzkiego: Łódź, Poland, 2005.
12. Madej, M.; Marczevska-Boczkowska, K.; Ozimina, D. Effect of tungsten on the durability of diamond-like carbon coatings in the chemical industry. *Przemysł Chem.* **2014**, *93*, 500–505.
13. Madej, M.; Ozimina, D.; Kurzydłowski, K.; Płociński, T.; Wieciński, P.; Styp-Rekowski, M.; Matuszewski, M. Properties of diamond-like carbon coatings deposited on CoCrMo alloys. *Trans. FAMENA* **2015**, *39*, 79–88.
14. Madej, M.; Ozimina, D. Electroless Ni-P-Al₂O₃ composite coatings. *Kovove Mater.* **2006**, *44*, 291–296.
15. Radek, N.; Szczotok, A.; Gądek-Moszczak, A.; Dwornicka, R.; Bronček, J.; Pietraszek, J. The impact of laser processing parameters on the properties of electro-spark deposited coatings. *Arch. Metall. Mater.* **2018**, *63*, 809–816.
16. Radhakrishnan, R.M.; Ramamoorthi, V.; Srinivasan, R. Wear characteristics of additively manufactured AlSi₁₀Mg against EN-31 and silicon carbide abrasive sheet counter bodies using box Behnken design approach. *Proc. Inst. Mech. Eng. Part L J. Mater. Des. Appl.* **2021**, *236*, 779–786. [[CrossRef](#)]
17. Chakkravarthy, V.; Jose, S.P.; Lakshmanan, M.; Manojkumar, P.; Lakshmi Narayan, R.; Kumaran, M. Additive manufacturing of novel Ti₋₃₀Nb₋₂Zr biomimetic scaffolds for successful limb salvage. *Mater. Today Proc.* **2022**, *64*, 1711–1716. [[CrossRef](#)]
18. Kumar, N.; Sharma, A.; Manoj, M.K.; Ahn, B. Taguchi optimization of tribological properties and corrosion behavior of self-lubricating Al–Mg–Si/MoS₂ composite processed by powder metallurgy. *J. Mater. Res. Technol.* **2023**, *26*, 1185–1197. [[CrossRef](#)]

19. Kozior, T.; Mamun, A.; Trabelsi, M.; Sabantina, L. Comparative Analysis of Polymer Composites Produced by FFF and P3J 3D Printing and Electrospinning Technologies for Possible Filter Applications. *Coatings* **2022**, *12*, 48. [CrossRef]
20. Piotrowska, K.; Madej, M.; Ozimina, D. Assessment of the Functional Properties of 316L Steel Alloy Subjected to Ion Implantation Used in Biotribological Systems. *Materials* **2021**, *14*, 5525. [CrossRef] [PubMed]
21. Milewski, K.; Kudliński, J.; Madej, M.; Ozimina, D. The interaction between diamond like carbon (DLC) coatings and ionic liquids under boundary lubrication conditions. *Metallurgija* **2017**, *1–2*, 55–58.
22. Ali, E.; Jean, M.M. Superior wear resistance of diamond and DLC coating. *Curr. Opin. Solid State Mater. Sci.* **2018**, *22*, 243–254. [CrossRef]
23. Naoto, O.; Masanori, H.; Kazuhiro, K.; Akasaka, H.; Tsujioka, M.; Harakuri, K.; Hirata, A.; Ohana, T.; Inaba, H.; Kano, M.; et al. Properties and Classification of Diamond-Like Carbon Films. *Materials* **2021**, *14*, 315. [CrossRef]
24. Zaki, A.; Faheemuddin, P.; Naila, R.M.; Ayesha, S. Effect of sandblasting, annealing and hydrophobic treatment on the nano-mechanical and corrosion behaviour of n-TiO₂-coated 316L stainless steel. *Curr. Sci. Assoc.* **2016**, *110*, 353–362. Available online: <https://www.jstor.org/stable/24906780> (accessed on 4 August 2023).
25. Poreba, M.; Reichert, M.; Sieniawski, J.; Zawadzka, P. Evaluation of DLC coating on IN 718 alloy produced by glow discharge plasma assisted CVD method. *Inżynieria Mater.* **2014**, *4*, 35.
26. Chakkravarthy, V.; Manojkumar, P.; Lakshmanan, M.; Eswar Prasad, K.; Dafale, R.; Chitra Vadhana, V.; Narayan, R.L. Comparing bio-tribocorrosion of selective laser melted Titanium-25% Niobium and conventionally manufactured Ti-6Al-4 V in inflammatory conditions. *J. Alloys Compd.* **2023**, *952*, 169852. [CrossRef]
27. Jastrzębski, K.; Jastrzębska, A.; Bociaga, D. A review of mechanical properties of Diamond-Like Carbon coatings with various dopants as candidates for biomedical applications. *Acta Innov.* **2017**, *22*, 40–57.
28. Chodun, R.; Skowronski, L.; Trzcinski, M.; Nowakowska-Langier, K.; Kulikowski, K.; Naparty, M.; Radziszewski, M.; Zdunek, K. The Amorphous Carbon Thin Films Synthesized by Gas Injection Magnetron Sputtering Technique in Various Gas Atmospheres. *Coatings* **2023**, *13*, 827. [CrossRef]
29. Meng, Y.; Xu, J.; Ma, L.; Jin, Z.; Prakash, B.; Ma, T.; Wang, W. A review of advances in tribology in 2020–2021. *Friction* **2022**, *10*, 1443–1595. [CrossRef]
30. Chronowska, K.; Kot, M.; Major, Ł. *Analysis of the Properties of New Groups of Coatings Applied in Highly Loaded Machine Components; Zeszyty Naukowe Politechniki Śląskiej: Gliwice, Poland, 2014; Volume 82, pp. 41–49.*
31. Vetter, J. 60 years of DLC coatings: Historical highlights and technical review of cathodic arc processes to synthesize various DLC types, and their evolution for industrial applications. *Surf. Coat. Technol.* **2014**, *257*, 213–240. [CrossRef]
32. Madej, M.; Ozimina, D.; Gałuszka, R.; Gałuszka, G. Corrosion, friction and wear performance of diamond like carbon coating. *Metallurgija* **2016**, *55*, 679–682.
33. Peng, J.; Huang, J.; Qiu, X.; Xiao, Y. Friction and wear performance of hydrogenated diamond-like coatings with non-metal element complex dopants against alumina in ambient air. *Wear* **2023**, *514–515*, 204571. [CrossRef]
34. Michalczewski, R.; Kalbarczyk, M.; Mańkowska-Snopczyńska, A.; Wieczorek, A. The Effect of a Gear Oil on Abrasion, Scuffing, and Pitting of the DLC-Coated 18CrNiMo7-6 Steel. *Coatings* **2018**, *9*, 2. [CrossRef]
35. Derakhshandeh, M.R.; Eshraghi, M.J.; Javaheri, M.; Khamseh, S. Diamond-like Carbon-Deposited Films: A New Class of Bio-Corrosion Protective Coatings. *Surf. Innov.* **2018**, *6*, 266–276. [CrossRef]
36. Batory, D.; Jędrzejczak, A.; Sobczyk-Guzenda, A.; Szymański, W.; Niedzielski, P. Studies of thermal stability of a-C:H:Si coatings produced by radio-frequency plasma assisted chemical vapour deposition (RF-PACVD) method. *Inżynieria Mater.* **2016**, *37*, 178–183. [CrossRef]
37. Kim, M.G.; Lee, K.R.; Eun, K.Y. Tribological behavior of silicon-incorporated diamond-like carbon films. *Surf. Coating. Technol.* **1999**, *112*, 204–209. [CrossRef]
38. Milewski, K.; Piotrowska, K.; Madej, M. Assessment of the properties of diamond-like carbon coatings (DLC) used in the lime industry. *Metallurgija* **2024**, *63*, 81–84.
39. Malisz, K.; Świeczko-Żurek, B.; Sionkowska, A. Preparation and Characterization of Diamond-like Carbon Coatings for Biomedical Applications—A Review. *Materials* **2023**, *16*, 3420. [CrossRef] [PubMed]
40. Bai, M.; Yang, L.; Li, J.; Lou, L.; Sun, S.; Inkson, B. Mechanical and tribological properties of Si and W doped diamond like carbon (DLC) under dry reciprocating sliding conditions. *Wear* **2021**, *484–485*, 204046. [CrossRef]
41. Dipen, K.R.; Ashwini, K.; Ajit, B.; Pradeep, L.M. Diamond-Like Carbon (DLC) Coatings: Classification, Properties, and Applications. *Appl. Sci.* **2021**, *11*, 4445. [CrossRef]
42. Ćorić, D.; Šnajdar Musa, M.; Sakoman, M.; Alar, Ž. Analysis of Different Complex Multilayer PACVD Coatings on Nanostructured WC-Co Cemented Carbide. *Coatings* **2021**, *11*, 823. [CrossRef]
43. Chayauski, V.; Zhylinski, V.; Kazachenko, V.; Tarasevich, A.; Taleb, A. Structural and Mechanical Properties of DLC/TiN Coatings on Carbide for Wood-Cutting Applications. *Coatings* **2023**, *13*, 1192. [CrossRef]
44. Chan, K.S.; Koike, M.; Okabe, T. Modeling wear of cast Ti alloys. *Acta Biomater.* **2007**, *3*, 383–389. [CrossRef] [PubMed]
45. Revankar, G.D.; Shetty, R.; Rao, S.S.; Gaitonde, V.N. Wear resistance enhancement of titanium alloy (Ti-6Al-4V) by ball burnishing process. *J. Mater. Res. Technol.* **2017**, *6*, 13–32. [CrossRef]

46. Available online: <https://www.oerlikon.com/balzers/be/en/portfolio/surface-technologies/pacvd/> (accessed on 22 July 2023).
47. Barnat Hunek, D. *Swobodna Energia Powierzchniowa Jako Czynniki Kształtujący Skuteczność Hydrofobizacji w Ochronie Konstrukcji Budowlanych*; Monografia; Wydawnictwo Politechniki Lubelskiej: Lublin, Poland, 2016.

Disclaimer/Publisher's Note: The statements, opinions and data contained in all publications are solely those of the individual author(s) and contributor(s) and not of MDPI and/or the editor(s). MDPI and/or the editor(s) disclaim responsibility for any injury to people or property resulting from any ideas, methods, instructions or products referred to in the content.